Ensemble statistics of bedload transport. Part 2: Stress history effects

Sophie Bodek[1], Dong Wang[2], Mark D. Shattuck[3], Corey S. O'Hern[2,4,5], Nicholas T. Ouellette[1]

[1]Department of Civil and Environmental Engineering, Stanford University, Stanford, CA 94305
[2]Department of Mechanical Engineering, Yale University, New Haven, CT 06520
[3]Benjamin Levich Institute and Physics Department, The City College of New York, New York, NY 10031
[4]Department of Applied Physics, Yale University, New Haven, CT 06520
[5]Department of Physics, Yale University, New Haven, CT 06520

Key Points:

- We use laboratory experiments to examine ensemble statistics of bedload trajectories subject to fluid flows from different directions
- Statistics describing the bulk sediment bed and individual grain tracks both systematically vary with direction of prior fluid flow
- Trackwise grain motion metrics (e.g., flight time and distance) converge to "unconditioned" values for Shields stress in excess of critical

Corresponding author: Sophie Bodek, `sbodek@stanford.edu`

Abstract

Bedload transport occurs when fluid shear stress becomes strong enough to entrain sediment. Recent studies show that the threshold for entrainment varies with the history of applied shear, with beds strengthening under sustained unidirectional flows and weakening when the flow direction is reversed. While stochastic bedload transport models incorporate variability in estimating the onset of grain motion, they typically do not consider time dependence. Here, we investigate how directional stress history affects the ensemble statistics of bedload motion using a rotating sediment bed in a laboratory flume. We subject a uniform sand bed to an initial subcritical conditioning flow, then rotate the bed to angular offsets of 0°, 45°, 90°, 135°, or 180° before applying erosive flows at Shields stresses ranging from 0.78 to 1.53 times the nominal critical value. Using high-resolution imaging, we identify individual grain trajectories and extract statistics associated with entrainment probability, grain activity, velocity, flight distance, and travel time. Bedload motion statistics vary systematically with prior flow direction: unidirectional conditioning (0°) reduces grain activity while producing slower, more abrupt grain flights, whereas reversed conditioning (135°–180°) results in the opposite outcome. We find that bulk bed statistics—grain activity and entrainment probability—retain signatures of directional stress history across all Shields stresses tested, while trackwise statistics—flight distance and travel time—converge toward unconditioned values above the critical shear. These results indicate that stress history primarily modulates the entrainment probability rather than altering the kinematics of grains undergoing sustained transport, with implications for stochastic bedload models.

Plain Language Summary

When flowing water mobilizes sediment grains on the surface of a sand or gravel bed, the ease of grain movement depends not only on the current flow conditions, but also on the history of previous flows. Recent studies show that sustained flows from the same direction can strengthen a sediment bed, making it harder to erode, while reversing the flow direction can weaken the bed and facilitate erosion. It remains unclear how this "stress history" effect alters the sediment bed, and whether individual grain flights are impacted. In this study, we examine how the direction of previous flows affects the probability distributions that characterize grain motion, such as how fast and far they travel before stopping. We use a laboratory flume with a rotating sand bed to control flow direction history, then use high-resolution images to identify individual grain trajectories. We find that flow history affects both the number of active grains and their individual flight characteristics near the onset of sediment motion. However, once flows are strong enough to sustain vigorous transport, the effect on individual grain flights disappears—only the number of moving grains and their pickup probability continue to reflect the bed's prior flow history.

1 Introduction

Bedload transport, the movement of sediment grains near the surface of a sand or gravel bed through rolling, sliding, and hopping motions, is a fundamental process that shapes fluvial, coastal, and aeolian landscapes. The accurate prediction of bedload transport rates has broad implications for water quality management, aquatic habitat assessment, and infrastructure safety. The conventional framework for predicting the onset of sediment motion relies on the Shields stress, τ_*, which represents the ratio of fluid-imposed bed shear stress to buoyancy-reduced gravitational stress (Shields, 1936). When the Shields stress approaches a critical value, τ_{*cr} (a "threshold of motion" that also varies with on particle Reynolds number), sediment grains begin to be mobilized into bedload transport as the forces imposed by a shearing flow overcome those resisting entrainment (e.g., Wiberg & Smith, 1987; Dey, 1999). Although this framework is widely used in bedload transport models (e.g., Meyer-Peter & Müller, 1948; Engelund & Fredsøe, 1976; Ashida & Michiue, 1973; Luque & Van Beek, 1976; Wong & Parker, 2006), challenges emerge due to the wide range of reported critical shear stresses at the onset of transport in both field and flume studies (Buffington & Montgomery, 1997) and the reduced predictive power of deterministic transport equations near the threshold of grain motion (Recking et al., 2012).

Predicting the onset of motion in fluid-driven granular beds is challenging due to factors such as the variable configuration of the sediment bed (Kirchner et al., 1990) and turbulent fluctuations in the overlying flow (Einstein & El-Samni, 1949), so that the physical mechanisms driving entrainment and transport are highly stochastic across spatial and temporal scales (Cameron et al., 2020; Diplas et al., 2008; Escauriaza et al., 2023; Papanicolaou et al., 2001; Sumer et al., 2003). Statistical descriptions of bedload motion have therefore been developed to parameterize sediment transport in probabilistic models (e.g., Schumer et al., 2009; Fan et al., 2016, 2014). This stochastic approach, initially developed by Einstein (1950) and Kalinske (1947), has been significantly advanced in recent decades through high-speed imaging and automated particle tracking techniques that permit large-scale data collection of individual and collective particle motion (Lajeunesse et al., 2010; Roseberry et al., 2012; Fathel et al., 2015; Salevan et al., 2017; Liu et al., 2019; Shim & Duan, 2017, 2019; Campagnol et al., 2013). These stochastic models are advantageous in that they are capable of parameterizing intermittency at near-threshold conditions (Benavides et al., 2022) and are computationally efficient compared to direct numerical simulations of coupled fluid-particle dynamics (Schmeeckle & Nelson, 2003; Schmeeckle, 2014; Durán et al., 2012; González et al., 2017; Escauriaza et al., 2023).

In addition to the variability inherent in the transport dynamics of individual grains, the macroscale properties of the bulk sediment bed vary in time. Observations of both experimental and natural systems find that τ_{*cr} varies with the history of fluid stress imparted onto the sediment bed (e.g., Mao, 2018; Turowski et al., 2011). The term "stress history" (also occasionally called "memory stress") generally describes the effects of subthreshold flows applied to a sediment bed and incorporates both the duration and magnitude of prior fluid stress (Monteith & Pender, 2005). These subcritical flows are typically referred to as "antecedent flows" (e.g., Monteith & Pender, 2005; A.-M. Ockelford & Haynes, 2013) or "conditioning flows" (e.g., An et al., 2021; Galanis et al., 2022).

Previous research investigating stress history effects has consistently shown that sediment beds exhibit strengthening behavior when subjected to unidirectional fluid shear, even without entraining grains into the flow (Haynes & Pender, 2007; Masteller & Finnegan, 2017; Masteller et al., 2019; Monteith & Pender, 2005; Oldmeadow & Church, 2006; A.-M. Ockelford & Haynes, 2013; Reid et al., 1985; Paphitis & Collins, 2005; A. Ockelford et al., 2019; An et al., 2021; Yang et al., 2024; Charru et al., 2004; Galanis et al., 2022; Bodek, Wang, Shattuck, O'Hern, & Ouellette, 2026a). This strengthening manifests as an increase in the critical Shields stress and a reduction in bedload transport rates, and can be considered as a form of strain hardening (Cúñez et al., 2022). The exact mechanism by which granular beds strengthen—or become hardened—is contested, with different mechanisms likely dominating depending on unique conditions of the sediment bed and overlying flow. One such manifestation of this phenomenon is seen in polydisperse granular systems as "armoring", where fluid stress below the critical value for the bulk system can first entrain finer grains, leaving only coarser grains that are more resistant to erosion and require larger fluid stresses for mobilization (Dietrich et al., 1989; Ferdowsi et al., 2017). Even in uniform sediment beds or polydisperse beds without measurable sediment transport, fluid shear can give rise to velocity fluctuations and subtle reorientation of the grains themselves, leading to more stable grain configurations, compaction, and thus strengthening of the bed (A.-M. Ockelford & Haynes, 2013; Masteller & Finnegan, 2017; Allen & Kudrolli, 2018). Additionally, as the bed experiences directional boundary shear, grain contacts can be preferentially loaded, forming anisotropic force chains that bear internal stresses and stabilize the material in the direction of the shear—a phenomenon known as shear jamming (Bi et al., 2011; Cates et al., 1998; Behringer & Chakraborty, 2018; Majmudar & Behringer, 2005). These preferentially loaded contact networks are fragile, however, and susceptible to disruption when the direction of fluid shear changes.

The presence of both isotropic (compaction) and anisotropic (shear jamming) mechanisms of strain hardening are supported by studies that observe bed weakening (i.e., lower $\tau_{*\,cr}$ or increased bedload transport) when the flow direction is reversed relative to the initial conditioning flow (Galanis et al., 2022; Cúñez et al., 2022; Bodek, Wang, Shattuck, O'Hern, & Ouellette, 2026a). Furthermore, in systems undergoing cyclic shear, the grain network must rearrange when the direction of the applied shear changes, further weakening the granular fabric (Slotterback et al., 2012). This effect was observed by Cúñez et al. (2022), who found that the granular fabric that developed from an oscillating flow was weaker than the anisotropic fabric developed under unidirectional flow, despite greater compaction of the bed material. Recent experimental work (Bodek, Wang, Shattuck, O'Hern, & Ouellette, 2026a) and discrete element method (DEM) simulations (Wang et al., 2026) examined sediment beds exposed to multiple directions of fluid shear, finding that strengthening occurs when conditioning and erosive flows originate from the same or similar directions (0° to 45° angular offsets), while weakening occurs when flows are reversed or nearly reversed (180° to 135° offsets).

While the individual and collective behavior of sediment grains are described by statistical ensembles in stochastic models of bedload transport, few studies examining stress history use probability distributions to characterize grain motion on the surface of a conditioned bed. Those that do typically use distributions of "bulk" metrics (i.e., parameters based on the collective behavior of all grains) such as grain activity, instantaneous grain velocity, or even volume fraction (Galanis et al., 2022; Bodek, Wang, Shattuck, O'Hern, & Ouellette, 2026a; Charru et al., 2004; Wang et al., 2026; Allen & Kudrolli, 2017). The influence of stress history on "trackwise" statistics (i.e., metrics determined from the identification of individual grain trajectories), such as grain flight distance, travel time, or grain rest time, has received even less attention. The characterization of these trackwise statistics, however, is valuable for calibrating stochastic bedload transport models and for estimating sediment flux, particularly for the advection-diffusion "entrainment form" of sediment flux that relies on a particle entrainment rate E, and the mean $\langle L_x \rangle$ and variance $\sigma^2_{L_x}$ of flight distance (Einstein, 1950; Furbish et al., 2012). Despite this significance, stochastic formulations for estimating bedload transport rarely incorporate time dependent dynamics. Furthermore, it is still unknown whether well-accepted probability distributions for grain motion parameters remain valid when sediment beds have been subjected to directional stress history, and whether the distribution parameters themselves encode information about the anisotropic fabric developed during conditioning flows.

The primary objective of this study is to investigate how directional stress history affects the ensemble statistics describing bedload motion. In a companion paper (Bodek, Wang, Shattuck, O'Hern, & Ouellette, 2026b), we examine the probability distributions of bulk and trackwise grain statistics for fluid shear stresses ranging from below the onset of grain motion to well in excess of the critical Shields stress. Here, we build upon the experimental framework of Bodek, Wang, Shattuck, O'Hern, and Ouellette (2026a), who demonstrated that bulk transport metrics depend on the angular offset between conditioning and erosive flows, and extend this analysis to examine the probability distributions characterizing trackwise grain motion parameters, including grain flight distance and travel time. Specifically, we address the following questions: (1) How does directional stress history affect the probability distributions and corresponding statistical parameters of grain activity, grain velocity, flight distance, and flight travel time? And (2) are the effects of stress history primarily manifested in the collective behavior of the bulk bed material (e.g, number of active grains) or in the kinematic parameters identified through grain trajectories (e.g., flight distances), or do they appear in both?

To address these questions, we carried out experiments in a laboratory flume where the sediment bed was subjected to an initial subcritical conditioning flow followed by an erosive flow from an offset direction. Using high-speed imaging and automated particle tracking, we extracted trajectories of individual sand grains and implemented a hidden Markov model (HMM) to segment these tracks into periods of motion and rest. From the segmented trajectories, we generate probability distributions for grain activity, velocity, flight distances, and travel times. We also identify the probability of entrainment and disentrainment using the HMM transition matrix. Our results confirm that bedload transport can be reduced or enhanced based on the history of directional fluid shear; however, the trackwise variables of grain flight distance and travel time do not preserve evidence of stress history for flows sufficiently above the onset of grain motion. By characterizing how fundamental probability distributions for bedload motion parameters vary with stress history, we provide a framework for incorporating temporal effects into stochastic sediment transport models.

2 Methods

2.1 Experimental Configuration and Procedure

Experiments were conducted by Bodek, Wang, Shattuck, O'Hern, and Ouellette (2026a) in an open channel flume at the Environmental Fluid Mechanics Laboratory at Stanford University. We direct the reader to this work as well as to O'Riordan et al. (1993) for a full description of the flume facility. The experimental configuration is also summarized in the companion paper (Bodek, Wang, Shattuck, O'Hern, & Ouellette, 2026b), and an abbreviated description is included here.

Experiments were conducted in a recirculating, open-channel flume with a 3 m long by 0.6 m wide rectangular test section. An inset sediment bed was installed into the floor of the glass-walled test section. This sediment bed was contained in a circular dish that was 45.7 cm (18 in) in diameter and 7.6 cm (3 in) deep. The sediment bed was mounted on a rotating turntable base, permitting multiple orientations of the sand bed relative to the flow direction. The sediment bed consisted of uniform medium to coarse-sized quartz sand (median grain size $D_{50} = 0.495$ mm; mass density $\rho_s = 2650$ kg/m^3).

A downward-facing camera was mounted above the center of the sediment bed to record the motion of sand grains through a small glass window that was used to minimize distortions in the flow surface. An acoustic Dopper profiling velocimeter (ADV) was positioned behind this window over the downstream portion of the sediment bed to collect fluid flow velocity measurements, which were used to characterize friction velocity u_*, bed stress τ_b, and Shields stress $\tau_* = \tau_b/[(\rho_s - \rho)gD_{50}]$, where $\rho = 1000$ kg/m^3 is the fluid density and g is the gravitational acceleration. The flow was hydraulically transitional, with particle Reynolds numbers $Re_p = u_* D_{50}/\nu$ ranging from $Re_p = 6.8$–10.6; the kinematic viscosity of water is approximately $\nu = 10^{-6}$ m^2/s. These flow conditions correspond to the bedload transport regime and the grains were not observed to travel in suspension during these experiments.

We prepared the sediment bed prior to each experiment using the same protocol. We first agitated the submerged sand bed using a stirring implement, then leveled the sediment bed by dragging a stiff piece of mesh over its surface in the downstream direction. For all experimental cases except the control, we subjected the sand bed to a 20 min subcritical conditioning flow. This conditioning flow had a Shields number that was approximately 75 to 80% of the nominal critical value for our sediment bed, which was determined to be $\tau_{*\,cr} \approx 0.033$ by comparison with the Shields curve. Significant grain motion did not occur during the conditioning, although grains were observed to jiggle in place and even roll one or two grain diameters. Following the conditioning flow, we rotated the sediment bed to one of five angular orientations (0°, 45°, 90°, 135°, and 180°) relative to the initial conditioning flow direction, where 0° represents the same direction as the conditioning flow and 180° represents the reversed direction. We note that the experimental procedure described in the companion paper does not include the 20 min conditioning flow (Bodek, Wang, Shattuck, O'Hern, & Ouellette, 2026b); this "unconditioned" case is used as the control here. Next, the flow rate was increased in a series of 9 settings of the variable speed pump from below to above the onset of grain motion where bedload transport was readily observed (i.e. from $\tau_*/\tau_{*\,cr} = 0.78$ to 1.53). After each increment, the flow was allowed to stabilize for 1 min, after which a 45 sec video of the sediment motion was collected. The bed was always reset before any new experiment was conducted; thus, observations of sediment motion were made on a newly prepared bed. Eight replicate trials were conducted for each of the six experimental conditions—the control and five angular orientations.

2.2 Imaging, Tracking, and Segmenting Sediment Grain Motion

The grain motion was imaged using a downward-facing camera at 120 frames per second with a 0.085 mm/pixel resolution. The camera was mounted above the center of the sediment bed and captured a 10.9 cm × 8.75 cm field of view. A sub-population of grains (17/83 mixture by volume) was spray-painted fluorescent orange and illuminated with ultraviolet light to facilitate particle identification. Particle trajectories were reconstructed using the multiframe predictive tracking algorithm of Ouellette et al. (2006), with approximately 800 grains identified per frame. Grain velocities and accelerations were computed from the trajectories via convolution with smoothing and differentiating kernels (Mordant et al., 2004).

An advancement in comparison to previous studies of sediment transport is the implementation of a hidden Markov model to segment grain trajectories into periods of motion and rest. Typical threshold-based methods for automated identification of grain flights require the selection of velocity or distance-based thresholds, while identification of periods of rest frequently require a minimum rest time (e.g., Martin et al., 2012; Cecchetto et al., 2018; González et al., 2017). The selection of these thresholds is subjective, and yet impacts the shape of the resulting PDF of instantaneous streamwise grain velocities and can significantly impact subsequent statistical analyses (Wu et al., 2020; Salevan et al., 2017). The HMM approach overcomes these limitations by providing an unsupervised classification that adapts to local transport conditions. Additionally, the transition probability structure inherent to the HMM makes rapid state changes extremely unlikely, resulting in temporal smoothing of the velocity signal. Thus temporary low-velocity fluctuations (e.g., brief collisions with the sediment bed) can still be classified as part of a grain flight segment, while brief high-velocity fluctuations (e.g., stationary grains on average that jiggle in place) can be categorized as in the rest state.

Our HMM consists of two hidden states (rest and motion) characterized by transition probabilities between states, and emission probability distributions for observed velocities given each state. We model rest-state velocities with a Student's t-distribution centered at zero (capturing still grains and grains that are jiggling without sustained downstream motion), and motion-state velocities with an exponential distribution (consistent with theoretical and observed bedload velocity distributions) (Salevan et al., 2017; Furbish & Schmeeckle, 2013; Roseberry et al., 2012). For each video of the sediment bed, we trained a unique HMM using the Baum-Welch algorithm (Baum, 1972) to estimate model parameters, then used the Viterbi algorithm (Viterbi, 1967) to decode the most probable state sequence for each trajectory. We also adjusted the likelihood of each hidden state by setting a higher threshold for the motion state based on the posterior probabilities to better match visual observations of motion and rest. Additional implementation details are given in Bodek, Wang, Shattuck, O'Hern, and Ouellette (2026b).

From the HMM-classified trajectories, we extracted flight distances and durations based on the time difference and streamwise and spanwise grain displacement from the start to end of a motion segment. We only considered completed grain flights (i.e., grain flights that are bookended with the rest state) to avoid truncated flights that either left the field of view or whose trajectories were not completed. We also identified the instantaneous velocities of moving grains and number of active grains using segments of trajectories identified as belonging to the motion state.

3 Results

3.1 Probability of Grain Motion and Rest

The transition probabilities determined from the HMM provide direct estimates of the probabilities of grain entrainment $P(entrainment)$ (i.e., the likelihood that a grain transitions from the rest state to the motion state at the next timestep) and disentrainment $P(disentrainment)$ (i.e., the likelihood that a grain transitions from the motion state to the rest state) (Bodek, Wang, Shattuck, O'Hern, & Ouellette, 2026b). The entrainment probability generally increases as a function of Shields stress for all bed orientations; however, this trend breaks down for the lowest flow settings ($\tau_*/\tau_{*\,cr} = 0.78$ and 0.90), which have a higher likelihood of entrainment than would otherwise be expected (Figure 1a). We address this over-prediction of motion at sub-threshold flow conditions in Bodek, Wang, Shattuck, O'Hern, and Ouellette (2026b), noting that the two-state mixture model initialized for all flow settings results in over-allocation of grain velocities in the positive tail of the Student's t distribution relative to the exponential distribution that represents moving grains, especially at the lowest flow settings where very few grains are mobilized. While we correct this over-prediction in our subsequent analysis of grain activity, velocity, and hop kinematics by setting a higher likelihood of motion based on the posterior probabilities (i.e., the probability that an observation belongs to a hidden state), this adjustment does not alter the underlying transition matrix and entrainment probabilities seen in Figure 1a. The disentrainment probability exhibits complementary behavior, decreasing monotonically as a function of Shields stress (Figure 1c).

Both the entrainment and disentrainment probabilities show a clear dependence on the directional stress history. We find that the entrainment probability is mostly consistent with (and may even exceed) the $P(entrainment)$ of the control case for Shields stresses ranging from below to slightly in excess of the critical value ($\tau_*/\tau_{*\,cr} \leq 1.19$) (Figure 1b). However, it is difficult to conclusively compare directional $P(entrainment)$ estimates for sub- and near-threshold flows ($\tau_*/\tau_{*\,cr} < 1.03$), since (as discussed above) the two-state mixture model used to initialize the HMM over-predicts entrainment probability in this flow regime (Figure 1a). As the Shields stress further exceeds the critical value, we identify greater variation in entrainment probability for each orientation. For these more rapid flows above the onset of sediment motion, we generally find that the entrainment probability increases as a function of bed orientation, with the highest $P(entrainment)$ identified for reversed and near-reversed flows (180° and 135° orientations). We also note that when the erosive flow is offset by 135° to the conditioning flow, the bed appears more susceptible to erosion with greater entrainment probability than the full 180° reversal case for these Shields stresses farther above the onset of motion ($\tau_*/\tau_{*\,cr} = 1.36$ and 1.53).

The disentrainment probability shows the opposite trend: $P(disentrainment)$ decreases as a function of bed orientation (Figure 1d). That is, grains are less likely to be deposited in the reversed and near-reversed flow cases (180° and 135° orientations) when compared to the control. The unidirectional and near-unidirectional cases (0° and 45° orientations) exhibit elevated disentrainment probabilities (i.e., moving grains are more likely to be deposited) across nearly all Shields stresses, particularly at and below the

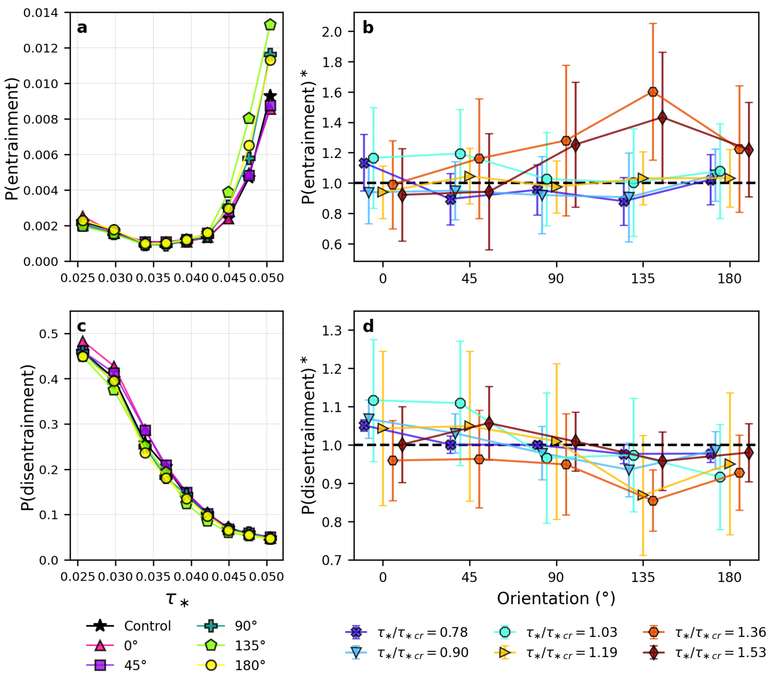

Figure 1. (a) Mean entrainment probability for each sediment bed orientation as identified by the HMM transition matrix, plotted as a function of Shields stress τ_*. (b) Mean entrainment probability normalized by that measured for the control condition, P(entrainment)*, plotted as a function of the angle between the conditioning flow and the subsequent erosive flow (i.e., the orientation angle) for several normalized Shields numbers $\tau_*/\tau_{*\,cr}$ near the critical value. Data points for each orientation are offset horizontally to assist with visualization. The horizontal dashed line corresponds to P(entrainment) $=$ 1; error bars indicate 95% confidence intervals computed for eight trials. (c) Mean disentrainment probability for each sediment bed orientation as identified by the HMM transition matrix, plotted as a function of Shields stress τ_*. (d) Mean disentrainment probability normalized by that measured for the control condition, P(disentrainment)*, plotted as a function of the angle between the conditioning flow and the subsequent erosive flow (i.e., the orientation angle) for several normalized Shields numbers $\tau_*/\tau_{*\,cr}$ near the critical value. The horizontal dashed line corresponds to P(disentrainment) $=$ 1; error bars indicate 95% confidence intervals computed for eight trials.

threshold of motion. This trend broadly applies across all bed stresses tested, although we note that disentrainment likelihood is elevated for sub-threshold conditions in the unidirectional and near-unidirectional cases, while the disentrainment likelihood is suppressed for above-threshold cases in the reversed and near-reversed flow directions (Figure 1d).

3.2 Grain Activity

We quantify grain activity by counting the number of active grains (i.e., grains in the motion state as designated by the HMM) in a given frame. We report this grain activity metric as an "activity fraction"—the ratio of moving grains to all grains identified in each frame. Similar activity metrics were used by Salevan et al. (2017) and Bodek, Wang, Shattuck, O'Hern, and Ouellette (2026b), while other studies use a grain activity normalized by unit surface area (Roseberry et al., 2012; Lajeunesse et al., 2010; Charru et al., 2004). The number of active grains provides a measure of the intensity of bedload transport. We show in Figure 2a that the activity fraction increases monotonically as a function of Shields stress for each bed orientation (control, 0°, 45°, 90°, 135°, and 180°), illustrating the transition from sporadic motion of a few grains at sub-critical conditions to sustained transport of a substantial fraction of identified grains above threshold.

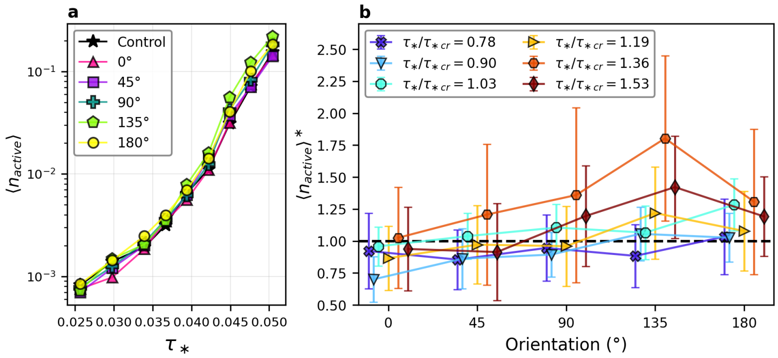

Figure 2. (a) Mean grain activity fraction $\langle n_{active} \rangle$ for each sediment bed orientation plotted as a function of Shields stress τ_*. (b) Mean activity fraction normalized by that measured for the control condition, $\langle n_{active} \rangle^*$, plotted as a function of the angle between the conditioning flow and the subsequent erosive flow (i.e., the orientation angle) for several normalized Shields numbers $\tau_*/\tau_{*\,cr}$ near the critical value. Data points for each orientation are offset horizontally to assist with visualization. The horizontal dashed line corresponds to $\langle n_{active} \rangle^* = 1$; error bars indicate 95% confidence intervals computed for eight trials.

Consistent with our results for entrainment probability (Section 3.1), grain activity shows clear dependence on directional stress history. We find that unidirectional conditioning (0° orientation) produces a systematically lower grain activity fraction across nearly the entire range of Shields stresses (Figure 2b); this reduction in grain activity is consistent with bed strengthening as fewer grains are mobilized under the same flow conditions. Generally, the activity fraction increases as a function of bed orientation angle, with the highest grain activity identified for reversed and near-reversed flows (180° and 135° orientations). We note that the activity fraction is more consistent with the control case for Shields stresses below and including the critical value ($\tau_*/\tau_{*\,cr} \leq 1.03$); as the Shields stress then exceeds this critical value, we identify greater variation in measurements for each orientation. For the unidirectional and near-unidirectional cases (0° and 45° orientations), the activity fraction does not deviate significantly from the control case for flows well in excess of the nominal critical value. However, at these faster flow settings, the activity fraction is persistently higher than for the control case for the reversed and near-reversed flow directions (180° and 135° orientations). We also note that when the erosive flow is offset by 135° to the conditioning flow, the bed appears weaker with more mobile grains than the full 180° reversal case for Shields stresses farther above the onset of motion ($\tau_*/\tau_{*\,cr} = 1.19$ to $\tau_*/\tau_{*\,cr} = 1.53$). This result is broadly consistent with Bodek, Wang, Shattuck, O'Hern, and Ouellette (2026a), who observed a persistent increase in grain activity for the reversed and nearly reversed flows (180° and 135° orientations) when compared to the unconditioned control case, particularly for bed stresses at and above the critical Shields stress.

3.3 Grain Velocities

Streamwise and spanwise grain velocity statistics were computed based on the probability density function (PDF) of instantaneous velocities of mobile grains (from categorization into the motion state by the HMM). We fit an exponential distribution to the PDF of instantaneous streamwise velocities u_g, as given by $P(u_g) = \frac{1}{\langle u_g \rangle} \exp\left[-\frac{u_g}{\langle u_g \rangle}\right]$, where $\langle u_g \rangle$ is the mean streamwise velocity. Similarly, we fit a two-sided exponential distribution to the instantaneous spanwise velocities v_g. Using the best-fit exponential distribution to determine the mean streamwise and spanwise grain velocity components for each bed stress, we find that both $\langle u_g \rangle$ and $\langle v_g \rangle$ (for $v_g > 0$ cm/s) increase as a function of Shields stress for all bed orientations (Figure 3a, 3c).

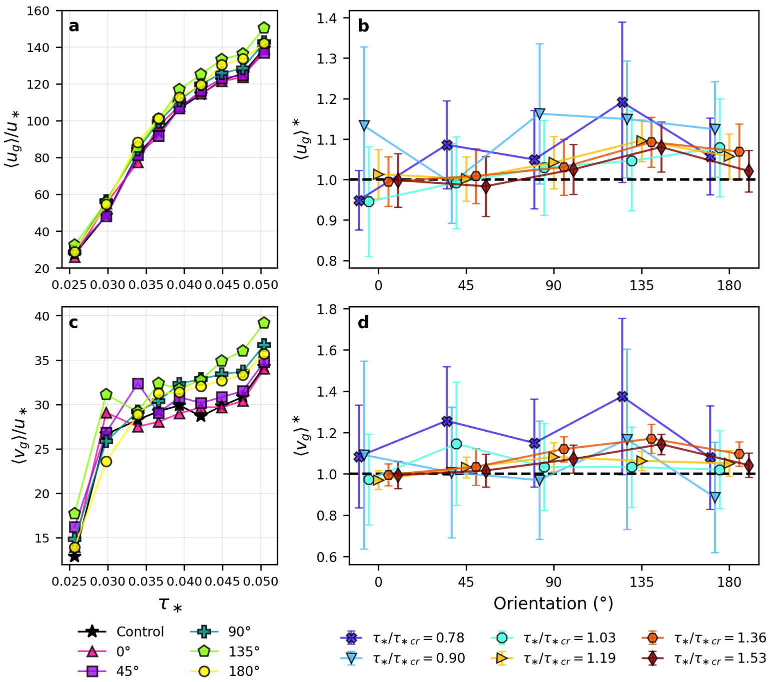

Figure 3. (a) Mean streamwise grain velocity normalized by friction velocity $\langle u_g \rangle / u_*$ for each sediment bed orientation plotted as a function of Shields stress τ_*; the normalizing factor u_* also increases as a function of τ_*. (b) Mean streamwise grain velocity normalized by that measured for the control condition, $\langle u_g \rangle^*$, plotted as a function of the angle between the conditioning flow and the subsequent erosive flow (i.e., the orientation angle) for several normalized Shields numbers $\tau_*/\tau_{*\,cr}$ near the critical value. Data points for each orientation are offset horizontally to assist with visualization. The horizontal dashed line corresponds to $\langle u_g \rangle^* = 1$; error bars indicate 95% confidence intervals computed for eight trials. (c) Mean spanwise grain velocity normalized by the friction velocity $\langle v_g \rangle / u_*$ for each sediment bed orientation plotted as a function of Shields stress τ_*. (d) Mean spanwise grain velocity normalized by that measured for the control condition, $\langle v_g \rangle^*$, plotted as a function of the angle between the conditioning flow and the subsequent erosive flow (i.e., the orientation angle) for several normalized Shields numbers $\tau_*/\tau_{*\,cr}$ near the critical value. The horizontal dashed line corresponds to $\langle v_g \rangle^* = 1$; error bars indicate 95% confidence intervals computed for eight trials.

When normalized by the unconditioned control case (Figure 3b), we broadly observe that the mean streamwise grain velocity increases as a function of orientation angle. This trend is most evident for bed stresses below and approaching the critical Shields stress, although we note considerable variation in individual measurements. As the flow settings exceed the threshold of grain motion, we note that the mean streamwise grain velocity becomes largely indistinguishable from the unconditioned control case for the unidirectional and near-unidirectional orientations (0° and 45° cases). However, we observe a faster mean grain velocity compared to the control for the reversed and near-reversed cases (180° and 135° orientations), as well as the perpendicular 90° case to a lesser extent. The faster velocities of grains at 90° to 180° orientations persist for nearly all flow settings. We also note that when the erosive flow is offset by from 135° to the conditioning flow, the bed appears weaker with higher mean grain velocities than the full 180° reversal case for many Shields stresses. This result is also consistent with Bodek, Wang, Shattuck, O'Hern, and Ouellette (2026a), who observed lower grain velocities below the critical Shields stress for the unidirectional case (0° orientation) and a persistent increase in streamwise grain velocity for reversed and nearly reversed flows (180° and 135° orientations), particularly for bed stresses at and above the critical Shields stress.

We observe similar behavior for the spanwise grain velocities when they are normalized by the unconditioned control (Figure 3d). For flow settings above the onset of motion, mean spanwise grain velocity becomes largely indistinguishable from the unconditioned control case for the unidirectional and near-unidirectional orientations (0° and 45° cases), but is faster than the control for the reversed and near-reversed cases (180° and 135° orientations), as well as the perpendicular 90° case to a lesser extent. The primary difference for spanwise velocities occurs below the critical Shields stress, where the mean velocity tends to be faster than the control for many bed orientations with high variation between individual experiments.

3.4 Grain Flight Times

Flight travel times T_f were determined using the PDF of the differences between the start and end times of trajectory segments categorized into the motion state by the HMM. We fit an exponential distribution to the PDF of flight travel times, given by $P(T_f) = \frac{1}{\langle T_f \rangle} \exp\left[-\frac{T_f}{\langle T_f \rangle}\right]$, to determine the mean duration of grain flights $\langle T_f \rangle$ at each bed stress. For all bed orientations (control, 0°, 45°, 90°, 135°, and 180°), mean flight time increases monotonically as a function of Shields stress (Figure 4a).

Directional stress history produces clear effects on mean flight time, particularly at and below the critical Shields stress. When normalized by the unconditioned control case (Figure 4b), we find that mean flight time increases as a function of orientation angle. The unidirectional flow orientation (0° offset) exhibits shorter flight durations below and approaching the threshold of motion, suggesting that grains in strengthened beds, once mobilized, return to rest more quickly. In this sub-threshold regime, longer flight times are measured for reversed and nearly-reversed flows (180° and 135° orientations). As the flow magnitude exceeds the critical Shields stress and approaches the highest setting ($\tau_*/\tau_{*\,cr} = 1.53$), mean flight times become indistinguishable from the unconditioned control case for all orientations of the sediment bed.

3.5 Grain Flight Distances

Streamwise and spanwise flight distance were determined using the PDF of grain displacements based on trajectory segments categorized into the motion state. We fit a Weibull distribution to the PDF of streamwise flight travel distances L_x, as given by $P(L_x) = \frac{k}{\lambda}\left(\frac{L_x}{\lambda}\right)^{k-1} \exp\left[-\left(\frac{L_x}{\lambda}\right)^{k}\right]$, where $k > 0$ is the shape parameter and $\lambda > 0$ is the scale parameter; the same distribution applies to spanwise flight distances L_y. Using the best-

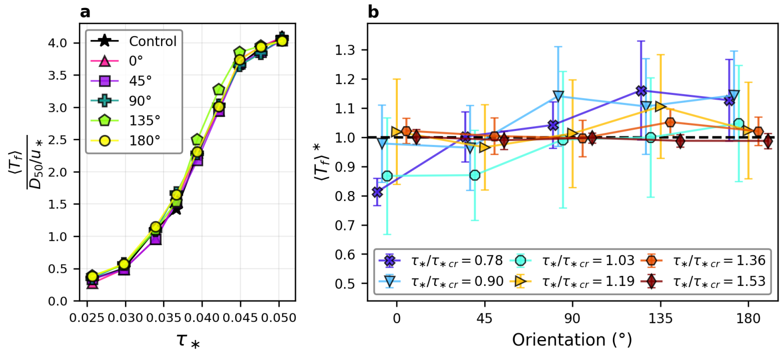

Figure 4. (a) Mean grain flight time $\langle T_f \rangle$ normalized by D_{50}/u_* for each sediment bed orientation plotted as a function of Shields stress τ_*. (b) Mean grain flight time normalized by that measured for the control condition, $\langle T_f \rangle^*$, plotted as a function of the angle between the conditioning flow and the subsequent erosive flow (i.e., the orientation angle) for several normalized Shields numbers $\tau_*/\tau_{*\,cr}$ near the critical value. Data points for each orientation are offset horizontally to assist with visualization. The horizontal dashed line corresponds to $\langle T_f \rangle^* = 1$; error bars indicate 95% confidence intervals computed for eight trials.

fit Weibull distribution, we determined the mean streamwise and spanwise flight distance: $\langle L_{x,\,y} \rangle = \lambda \Gamma\left(1 + \frac{1}{k}\right)$, where Γ is the gamma function. For all bed orientations (control, 0°, 45°, 90°, 135°, and 180°), both mean streamwise and spanwise flight distances increase monotonically as a function of Shields stress (Figure 5a, 5c).

Directional stress history produces systematic effects on grain flight distance that closely parallel those observed for flight time identified in Section 3.4. When normalized by the unconditioned control case (Figure 5b), we again broadly observe that the mean streamwise flight distance increases as a function of orientation angle. This trend is most evident for bed stresses below and approaching the critical Shields stress, although we note variation in individual measurements. As the fluid shear exceeds the threshold of grain motion, we note that the mean streamwise flight distance becomes largely indistinguishable from the unconditioned control case for the unidirectional, near-unidirectional, and perpendicular orientations (0°, 45°, and 90° cases). However, we observe longer mean grain flights compared to the control for the reversed and near-reversed cases (180° and 135° orientations). The longer flight distances for the 135° to 180° orientations persist for nearly all flow conditions. We also note that when the erosive flow is offset by 135° to the conditioning flow, the grains travel farther on average than the full 180° reversal case for many Shields stresses. This result agrees with the trends observed for grain velocity and mean flight time (Sections 3.3, 3.4).

We observe similar behavior for spanwise flight distances when normalized by the unconditioned control (Figure 5d). For fluid shear above the onset of motion, the mean distance traveled by spanwise grain flights becomes largely indistinguishable from the unconditioned control case for the unidirectional and near-unidirectional orientations (0° and 45° cases), but grains travel farther than the control for the perpendicular, near-reversed, and reversed cases (90° to 180° orientations). The primary difference when compared to streamwise flight distances occurs below the critical Shields stress. In the spanwise direction, grains tend to travel farther than the control for many bed orientations with high variation between individual experiments. This lack of directional effect on spanwise flight distance for sub-threshold conditions mirrors the results for the spanwise velocity.

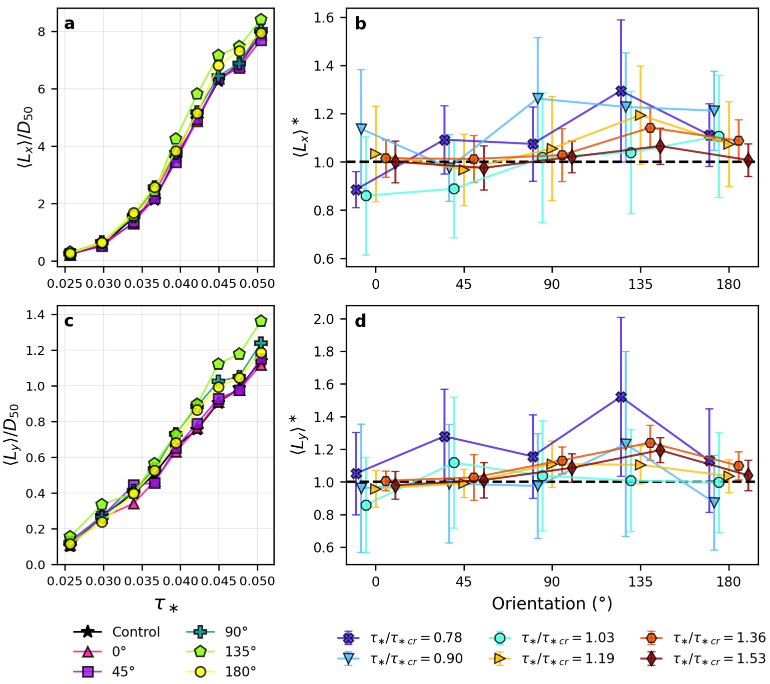

Figure 5. (a) Mean streamwise grain flight distance $\langle L_x \rangle$ normalized by the median grain size D_{50} for each sediment bed orientation plotted as a function of Shields stress τ_*. (b) Mean streamwise flight distance normalized by that measured for the control condition, $\langle L_x \rangle^*$, plotted as a function of the angle between the conditioning flow and the subsequent erosive flow (i.e., the orientation angle) for several normalized Shields numbers $\tau_*/\tau_{*\,cr}$ near the critical value. Data points for each orientation are offset horizontally to assist with visualization. The horizontal dashed line corresponds to $\langle L_x \rangle^* = 1$; error bars indicate 95% confidence intervals computed for eight trials. (c) Mean spanwise grain flight distance $\langle L_y \rangle$ normalized by the median grain size D_{50} for each sediment bed orientation plotted as a function of Shields stress τ_*. (d) Mean streamwise flight distance normalized by that measured for the control condition, $\langle L_y \rangle^*$, plotted as a function of the angle between the conditioning flow and the subsequent erosive flow (i.e., the orientation angle) for several normalized Shields numbers $\tau_*/\tau_{*\,cr}$ near the critical value. The horizontal dashed line corresponds to $\langle L_y \rangle^* = 1$; error bars indicate 95% confidence intervals computed for eight trials.

4 Discussion

Our results demonstrate that directional stress history—the angular offset between an initial conditioning flow and subsequent erosive flow—systematically affects ensemble statistics characterizing bedload transport. However, the nature and persistence of these effects differ fundamentally between the collective statistics of the bulk bed material (which we term bulk metrics) and the kinematic parameters identified from individual grain trajectories (trackwise metrics).

Bulk statistics that characterize the collective behavior of sediment grains show strong directional dependence that persists well above the nominal critical Shields stress. We consider activity fraction as well as entrainment and disentrainment probabilities, as parameters that fall under this population-level description. Because we use the segmented trajectories to designate the velocities of moving grains, we consider grain velocity a kinematic statistic associated with other trackwise parameters (namely grain flight distance and travel time), which are further discussed below. Unidirectional conditioning (0° offset) broadly reduces grain activity relative to the unconditioned control case; however, this strengthening effect fades once the fluid shear exceeds the onset of sediment motion (Figure 2b). Similarly, we identify a higher probability of disentrainment for sediment beds that have experienced a unidirectional conditioning flow, also noting that disentrainment probabilities approach the control case for flows in excess of the critical Shields stress (Figure 1d). Entrainment probability, meanwhile, does not appear to vary significantly from the unconditioned control case, particularly for flows above onset (Figure 1b). Thus, we find that the reduced number of mobile grains observed in sediment beds exposed to unidirectional fluid shear may be attributed to an increased likelihood of deposition below and near the onset of motion.

Conversely, conditioning by reversed and near-reversed flows (180° and 135° offsets) enhances grain activity and entrainment probability, particularly for flows above the threshold of motion. We observe that both grain activity and entrainment probability do not appear to vary significantly from the unconditioned control case for subcritical flows; however, once fluid shear exceeds the critical value for sediment mobilization, we identify persistent bed weakening through a higher likelihood of grain entrainment and thus more grains in motion (Figure 2b, 1b). We also note that, compared to the unconditioned control case, grains in reversed and near-reversed flows are less likely to be disentrained when experiencing transport by above-threshold flows (Figure 1d). This weakening effect is most prominent for the case where the erosive flow is offset by 135° to the conditioning flow. In contrast to the strengthening observed for the unidirectional flow case, we find that the signature of a weakened sediment bed persists above the onset of motion possibly due to collective entrainment effects; as more grains are mobilized, they may destabilize their neighbors leading to enhanced transport as has been observed in both unimodal (e.g., Ancey et al., 2006) and polydisperse granular beds (e.g., Galanis et al., 2021).

Trackwise statistics encompass kinematic parameters identified from individual grain trajectories, including the velocity of moving grains. These trackwise metrics also show a dependence on directional stress history, but only in the sub- and near-threshold regime. At subcritical and near-critical Shields stresses, unidirectional conditioning (0° offset) generally results in grains undergoing slower flights over shorter distances. This is seen in all our trackwise metrics, consisting of lower streamwise grain velocity (Figure 3b), grain flight time (Figure 4b), and streamwise flight distance (Figure 5b). Reversed and near-reversed conditioning flows (180° and 135° offsets) produce the opposite effect with faster, longer, more sustained grain flights. However, once the fluid shear exceeds the nominal critical value for sediment entrainment, these directional effects on trackwise statistics largely vanish, with all orientations converging toward the unconditioned control values. This convergence indicates that stress history primarily affects the characteristics of marginal grain motion near threshold, but has a diminishing influence on the kinematics of individual flights once transport is well-established. Interestingly, we note that while kinematic signals of directional stress history are largely suppressed at the highest fluid shear settings, grain velocities and flight distances tend to remain elevated for the 135° conditioning orientation, consistent with observations of bulk sediment bed metrics. It is unclear why the 135° orientation is consistently more erodible. One possible explanation is that the shear imparted onto the sediment bed from the bed leveling procedure produced a downstream-oriented directional fabric that persists for the 180° flow reversal, resulting in a slightly stronger 180° case compared to the 135° case. Another possibility is the ability of grains to more easily move around others that have been strengthened by the conditioning flow when the erosive flow is not completely reversed.

This dichotomy between bulk population-level effects and kinematic trackwise effects is broadly consistent with previous experimental studies but provides new mechanistic insight. Both Galanis et al. (2022) and Bodek, Wang, Shattuck, O'Hern, and Ouellette (2026a) found strengthening in sediment beds conditioned by unidirectional (0° offset) flows and weakening in beds conditioned by reversed flows (180° offset), as measured by statistical parameters extracted from the PDF of instantaneous streamwise velocity for all identified grains (both those in motion and at rest). DEM simulations by Wang et al. (2026) found that, for sediment beds subject to unidirectional fluid shear, grains at the bed surface settle into pockets aligned with the flow direction during conditioning. Such configurations create directionally dependent geometric stability: grains are harder to dislodge in the alignment direction but easier to dislodge in perpendicular or reversed directions. When mobilized near threshold, these aligned grains may travel shorter distances before encountering stable downstream pockets oriented similarly to their initial configuration. In the reversed 180° orientation, surface grains settle into pockets oriented opposite to the erosive flow, creating less stable configurations that, when disrupted, allow grains to travel farther before finding suitable deposition sites. However, as the Shields stress increases and transport becomes more sustained, the surface is continually reworked by mobile grains, erasing the directional signature of the conditioning flow. This "erasure" of stress history effects is consistent with observations of natural gravel-bed rivers. Bed stability increases and bedload transport decreases during drier times of year when streamflow is low and bankfull floods are uncommon; subsequently, during spring snowmelt or rainy periods when bankfull or greater floods tend to occur, these rapid flows disrupt any structure or orientation that may have developed and "reset" the bed to a more mobile and unstructured state (Masteller et al., 2019; Oldmeadow & Church, 2006; Vericat et al., 2006).

This distinction suggests that stress history operates through two complementary mechanisms. First, stress history modulates the ease of grain entrainment and disentrainment, affecting how readily grains transition between rest and motion states—an effect that persists across the sub- to above threshold transport regimes. Second, stress history affects the characteristics of grain motion once mobilized (velocity, distance, duration), but primarily in the intermittent sub-threshold transport regime where grain-bed interactions are most sensitive to subtle variations in bed configuration. Once transport is well-established above threshold, the dominant control on grain flight characteristics shifts from bed structure to flow forcing, and stress history signatures in individual trajectory kinematics fade. However, the continued influence of stress history on entrainment/disentrainment probabilities and grain activity indicates that population-level effects remain important even at higher transport intensities. This persistence of memory stress in the bulk sediment bed metrics may possibly be due to collective entrainment effects: as more grains are mobilized, they destabilize their neighbors leading to enhanced transport (Ancey et al., 2006). Alternately, in these cases where the direction of the erosive flow is reversed, the sand bed may develop a wider shear zone, thus experiencing greater disruption of grain contacts and increased sediment motion deeper into the subsurface (Slotterback et al., 2012; Toiya et al., 2004).

5 Conclusion

The primary objective of this study was to investigate how directional stress history affects the ensemble statistics of bedload transport. Specifically, we addressed two key questions: (1) How does directional stress history affect the probability distributions and associated statistical parameters of grain activity, velocity, flight distance, and flight travel time? And (2) are the effects of stress history primarily manifested in the collective statistics of the bulk bed material (bulk metrics), in the kinematic parameters identified through individual grain trajectories (trackwise metrics), or both? To address these questions, we conducted experiments in a laboratory flume using a rotating sediment bed apparatus that allowed us to impose directional stress history at offset angles of 0°, 45°, 90°, 135°, and 180° to the initial 20 min conditioning flow. Our results show that directional stress history affects both the bulk and trackwise statistics of bedload motion. We observe strengthening in the unidirectional case (0° offset) with reduced grain activity, greater likelihood of deposition, and slower, more abbreviated grain flights—especially at and below the nominal critical Shields stress. Conversely, we observe weakening in the reversed (180° offset) and nearly reversed (135° offset) cases with enhanced grain activity, higher entrainment probabilities, and faster, more sustained grain flights. While increased grain activity and likelihood of entrainment persist well above the threshold of motion for the reversed and near-reversed flow directions, the trackwise metrics of grain flight distance, time, and velocity approach those measured for the unconditioned control.

The transient nature of trackwise effects (velocity, distance, time) suggests a surface-level mechanism that becomes less relevant as transport intensity increases. We interpret this as evidence for directionally-dependent surface grain configurations—including grain pockets, protrusion angles, and local sheltering arrangements—that affect the trajectories of mobilized grains in the near-threshold regime. These findings have important implications for stochastic bedload transport models. Our results demonstrate that both the activity form and entrainment form parameterizations of sediment flux must account for directional stress history, as both the number of mobilized grains and their kinematic properties vary with the angular offset between historical and current flow directions. In natural systems where flow directions vary, the directional history of stress may significantly enhance or reduce transport rates beyond what would be predicted from the instantaneous fluid stress alone. By characterizing how the probability distributions describing grain motion characteristics vary with stress history, we provide a framework for incorporating these effects into stochastic sediment transport models.

Open Research Section

All experimental data and codes used to generate the figures in this paper are deposited in Figshare, a free and open repository. These datasets can be accessed using the following link: https://figshare.com/s/ec90be61ecd62ec3d049 (Bodek, Wang, Shattuck, O'Hern, & Ouellette, 2026).

Acknowledgments

Financial support was provided by the Army Research Office (ARO Award #W911NF-23-1-0032). The authors thank Stanford Research Computing for computational support via the Sherlock cluster. The authors declare no conflict of interest relevant to this study.

References

Allen, B., & Kudrolli, A. (2017). Depth resolved granular transport driven by shearing fluid flow. *Physical Review Fluids*, *2*(2), 024304.

Allen, B., & Kudrolli, A. (2018). Granular bed consolidation, creep, and armoring under subcritical fluid flow. *Physical Review Fluids*, *3*(7), 074305.

An, C., Hassan, M. A., Ferrer-Boix, C., & Fu, X. (2021, April). Effect of stress history on sediment transport and channel adjustment in graded gravel-bed rivers. *Earth Surf. Dyn.*, *9*(2), 333–350. doi: 10.5194/esurf-9-333-2021

Ancey, C., Böhm, T., Jodeau, M., & Frey, P. (2006, July). Statistical description of sediment transport experiments. *Phys. Rev. E*, *74*(1), 011302. doi: 10.1103/PhysRevE.74.011302

Ashida, K., & Michiue, M. (1973). Studies on bed-load transport rate in open channel flows. *IN: SEDIMENT TRANSPORTATION, VOLUME 1*.

Baum, L. E. (1972). An inequality and associated maximization technique in statistical estimation for probabilistic functions of markov processes. *Inequalities*,

3(1), 1–8.
Behringer, R. P., & Chakraborty, B. (2018, November). The physics of jamming for granular materials: a review. *Rep. Prog. Phys.*, *82*(1), 012601. doi: 10.1088/1361-6633/aadc3c
Benavides, S. J., Deal, E., Rushlow, M., Venditti, J. G., Zhang, Q., Kamrin, K., & Perron, J. T. (2022). The impact of intermittency on bed load sediment transport. *Geophysical Research Letters*, *49*(5), e2021GL096088.
Bi, D., Zhang, J., Chakraborty, B., & Behringer, R. P. (2011, December). Jamming by shear. *Nature*, *480*(7377), 355–358. doi: 10.1038/nature10667
Bodek, S., Wang, D., Shattuck, M. D., O'Hern, C. S., & Ouellette, N. T. (2026). Ensemble statistics of bedload transport: Dataset of grain motion and rest measurements. *figshare [dataset]*. doi: https://figshare.com/s/ec90be61ecd62ec3d049
Bodek, S., Wang, D., Shattuck, M. D., O'Hern, C. S., & Ouellette, N. T. (2026a). Anisotropic stress history effects in erodible sediment beds. *Journal of Geophysical Research: Earth Surface*, *131*(1), e2025JF008561.
Bodek, S., Wang, D., Shattuck, M. D., O'Hern, C. S., & Ouellette, N. T. (2026b). Ensemble statistics of bedload transport. Part 1: Grain motion at near-threshold conditions [manuscript submitted for publication].
Buffington, J. M., & Montgomery, D. R. (1997, August). A systematic analysis of eight decades of incipient motion studies, with special reference to gravel-bedded rivers. *Water Resour. Res.*, *33*(8), 1993–2029. doi: 10.1029/96WR03190
Cameron, S. M., Nikora, V. I., & Witz, M. J. (2020, April). Entrainment of sediment particles by very large-scale motions. *J. Fluid Mech.*, *888*, A7. doi: 10.1017/jfm.2020.24
Campagnol, J., Radice, A., Nokes, R., Bulankina, V., Lescova, A., & Ballio, F. (2013). Lagrangian analysis of bed-load sediment motion: database contribution. *Journal of Hydraulic Research*, *51*(5), 589–596.
Cates, M. E., Wittmer, J. P., Bouchaud, J.-P., & Claudin, P. (1998, August). Jamming, Force Chains, and Fragile Matter. *Phys. Rev. Lett.*, *81*(9), 1841–1844. doi: 10.1103/PhysRevLett.81.1841
Cecchetto, M., Tregnaghi, M., Bottacin-Busolin, A., Tait, S., Cotterle, L., & Marion, A. (2018). Diffusive regimes of the motion of bed load particles in open channel flows at low transport stages. *Water Resources Research*, *54*(11), 8674–8691.
Charru, F., Mouilleron, H., & Eiff, O. (2004, November). Erosion and deposition of particles on a bed sheared by a viscous flow. *J. Fluid Mech.*, *519*, 55–80. doi: 10.1017/S0022112004001028
Cúñez, F. D., Franklin, E. M., Houssais, M., Arratia, P., & Jerolmack, D. J. (2022, June). Strain hardening by sediment transport. *Phys. Rev. Res.*, *4*(2), L022055. doi: 10.1103/PhysRevResearch.4.L022055
Dey, S. (1999, May). Sediment threshold. *Appl. Math. Model.*, *23*(5), 399–417. doi: 10.1016/S0307-904X(98)10081-1
Dietrich, W. E., Kirchner, J. W., Ikeda, H., & Iseya, F. (1989). Sediment supply and the development of the coarse surface layer in gravel-bedded rivers. *Nature*, *340*(6230), 215–217.
Diplas, P., Dancey, C. L., Celik, A. O., Valyrakis, M., Greer, K., & Akar, T. (2008, October). The Role of Impulse on the Initiation of Particle Movement Under Turbulent Flow Conditions. *Science*, *322*(5902), 717–720. doi: 10.1126/science.1158954
Durán, O., Andreotti, B., & Claudin, P. (2012). Numerical simulation of turbulent sediment transport, from bed load to saltation. *Physics of Fluids*, *24*(10).
Einstein, H. A. (1950). *The bed-load function for sediment transportation in open channel flows* (Vol. 1026). US Government Printing Office.

Einstein, H. A., & El-Samni, E.-S. A. (1949, July). Hydrodynamic Forces on a Rough Wall. *Rev. Mod. Phys.*, *21*(3), 520–524. doi: 10.1103/RevModPhys.21.520

Engelund, F., & Fredsøe, J. (1976). A sediment transport model for straight alluvial channels. *Hydrology Research*, *7*(5), 293–306.

Escauriaza, C., González, C., Williams, M. E., & Brevis, W. (2023, March). Models of bed-load transport across scales: turbulence signature from grain motion to sediment flux. *Stochastic Environ. Res. Risk Assess.*, *37*(3), 1039–1052. doi: 10.1007/s00477-022-02333-9

Fan, N., Singh, A., Guala, M., Foufoula-Georgiou, E., & Wu, B. (2016). Exploring a semimechanistic episodic langevin model for bed load transport: Emergence of normal and anomalous advection and diffusion regimes. *Water Resources Research*, *52*(4), 2789–2801.

Fan, N., Zhong, D., Wu, B., Foufoula-Georgiou, E., & Guala, M. (2014). A mechanistic-stochastic formulation of bed load particle motions: From individual particle forces to the fokker-planck equation under low transport rates. *Journal of Geophysical Research: Earth Surface*, *119*(3), 464–482.

Fathel, S. L., Furbish, D. J., & Schmeeckle, M. W. (2015). Experimental evidence of statistical ensemble behavior in bed load sediment transport. *Journal of Geophysical Research: Earth Surface*, *120*(11), 2298–2317.

Ferdowsi, B., Ortiz, C. P., Houssais, M., & Jerolmack, D. J. (2017, November). River-bed armouring as a granular segregation phenomenon. *Nat. Commun.*, *8*(1363), 1–10. doi: 10.1038/s41467-017-01681-3

Furbish, D. J., Haff, P. K., Roseberry, J. C., & Schmeeckle, M. W. (2012, September). A probabilistic description of the bed load sediment flux: 1. Theory. *J. Geophys. Res. Earth Surf.*, *117*(F3). doi: 10.1029/2012JF002352

Furbish, D. J., & Schmeeckle, M. W. (2013, March). A probabilistic derivation of the exponential-like distribution of bed load particle velocities. *Water Resour. Res.*, *49*(3), 1537–1551. doi: 10.1002/wrcr.20074

Galanis, M., Shattuck, M. D., O'Hern, C. S., & Ouellette, N. T. (2022, January). Directional strengthening and weakening in hydrodynamically sheared granular beds. *Phys. Rev. Fluids*, *7*(1), 013802. doi: 10.1103/PhysRevFluids.7.013802

Galanis, M., Wang, P., Shattuck, M. D., O'Hern, C. S., & Ouellette, N. T. (2021, September). Onset of grain motion in eroding subaqueous bimodal granular beds. *Phys. Rev. Fluids*, *6*(9), 094301. doi: 10.1103/PhysRevFluids.6.094301

González, C., Richter, D. H., Bolster, D., Bateman, S., Calantoni, J., & Escauriaza, C. (2017, February). Characterization of bedload intermittency near the threshold of motion using a Lagrangian sediment transport model. *Environ. Fluid Mech.*, *17*(1), 111–137. doi: 10.1007/s10652-016-9476-x

Haynes, H., & Pender, G. (2007, April). Stress History Effects on Graded Bed Stability. *J. Hydraul. Eng.*, *133*(4), 343–349. doi: 10.1061/(ASCE)0733-9429(2007)133:4(343)

Kalinske, A. (1947). Movement of sediment as bed load in rivers. *Eos, Transactions American Geophysical Union*, *28*(4), 615–620.

Kirchner, J. W., Dietrich, W. E., Iseya, F., & Ikeda, H. (1990, August). The variability of critical shear stress, friction angle, and grain protrusion in water-worked sediments. *Sedimentology*, *37*(4), 647–672. doi: 10.1111/j.1365-3091.1990.tb00627.x

Lajeunesse, E., Malverti, L., & Charru, F. (2010, December). Bed load transport in turbulent flow at the grain scale: Experiments and modeling. *J. Geophys. Res. Earth Surf.*, *115*(F4). doi: 10.1029/2009JF001628

Liu, M. X., Pelosi, A., & Guala, M. (2019, November). A Statistical Description of Particle Motion and Rest Regimes in Open-Channel Flows Under Low Bedload Transport. *J. Geophys. Res. Earth Surf.*, *124*(11), 2666–2688. doi: 10.1029/2019JF005140

Luque, R. F., & Van Beek, R. (1976, April). Erosion and transport of bed-load sediment. *Journal of Hydraulic Research*. Retrieved from `https://www.tandfonline.com/doi/abs/10.1080/00221687609499677`
Majmudar, T. S., & Behringer, R. P. (2005, June). Contact force measurements and stress-induced anisotropy in granular materials. *Nature*, *435*(7045), 1079–1082. doi: 10.1038/nature03805
Mao, L. (2018, December). The effects of flood history on sediment transport in gravel-bed rivers. *Geomorphology*, *322*, 196–205. doi: 10.1016/j.geomorph.2018.08.046
Martin, R. L., Jerolmack, D. J., & Schumer, R. (2012). The physical basis for anomalous diffusion in bed load transport. *Journal of Geophysical Research: Earth Surface*, *117*(F1).
Masteller, C. C., & Finnegan, N. J. (2017, January). Interplay between grain protrusion and sediment entrainment in an experimental flume. *J. Geophys. Res. Earth Surf.*, *122*(1), 274–289. doi: 10.1002/2016JF003943
Masteller, C. C., Finnegan, N. J., Turowski, J. M., Yager, E. M., & Rickenmann, D. (2019, March). History-Dependent Threshold for Motion Revealed by Continuous Bedload Transport Measurements in a Steep Mountain Stream. *Geophys. Res. Lett.*, *46*(5), 2583–2591. doi: 10.1029/2018GL081325
Meyer-Peter, E., & Müller, R. (1948). Formulas for bed-load transport. In *Iahsr 2nd meeting, stockholm, appendix 2.*
Monteith, H., & Pender, G. (2005, December). Flume investigations into the influence of shear stress history on a graded sediment bed. *Water Resour. Res.*, *41*(12). doi: 10.1029/2005WR004297
Mordant, N., Crawford, A. M., & Bodenschatz, E. (2004, June). Experimental Lagrangian acceleration probability density function measurement. *Physica D*, *193*(1), 245–251. doi: 10.1016/j.physd.2004.01.041
Ockelford, A., Woodcock, S., & Haynes, H. (2019, November). The impact of inter-flood duration on non-cohesive sediment bed stability. *Earth Surf. Processes Landforms*, *44*(14), 2861–2871. doi: 10.1002/esp.4713
Ockelford, A.-M., & Haynes, H. (2013, June). The impact of stress history on bed structure. *Earth Surf. Processes Landforms*, *38*(7), 717–727. doi: 10.1002/esp.3348
Oldmeadow, D. F., & Church, M. (2006). A field experiment on streambed stabilization by gravel structures. *Geomorphology*, *78*(3-4), 335–350.
O'Riordan, C. A., Monismith, S. G., & Koseff, J. R. (1993, December). A study of concentration boundary-layer formation over a bed of model bivalves. *Limnol. Oceanogr.*, *38*(8), 1712–1729. doi: 10.4319/lo.1993.38.8.1712
Ouellette, N. T., Xu, H., & Bodenschatz, E. (2006, February). A quantitative study of three-dimensional Lagrangian particle tracking algorithms. *Exp. Fluids*, *40*(2), 301–313. doi: 10.1007/s00348-005-0068-7
Papanicolaou, A. N., Diplas, P., Dancey, C. L., & Balakrishnan, M. (2001, March). Surface Roughness Effects in Near-Bed Turbulence: Implications to Sediment Entrainment. *J. Eng. Mech.*, *127*(3), 211–218. doi: 10.1061/(ASCE)0733-9399(2001)127:3(211)
Paphitis, D., & Collins, M. B. (2005, August). Sand grain threshold, in relation to bed 'stress history': an experimental study. *Sedimentology*, *52*(4), 827–838. doi: 10.1111/j.1365-3091.2005.00710.x
Recking, A., Liébault, F., Peteuil, C., & Jolimet, T. (2012, June). Testing bedload transport equations with consideration of time scales. *Earth Surf. Processes Landforms*, *37*(7), 774–789. doi: 10.1002/esp.3213
Reid, I., Frostick, L. E., & Layman, J. T. (1985, January). The incidence and nature of bedload transport during flood flows in coarse-grained alluvial channels. *Earth Surf. Processes Landforms*, *10*(1), 33–44. doi: 10.1002/esp.3290100107
Roseberry, J. C., Schmeeckle, M. W., & Furbish, D. J. (2012, September). A prob-

abilistic description of the bed load sediment flux: 2. Particle activity and motions. *J. Geophys. Res. Earth Surf.*, *117*(F3). doi: 10.1029/2012JF002353

Salevan, J. C., Clark, A. H., Shattuck, M. D., O'Hern, C. S., & Ouellette, N. T. (2017, November). Determining the onset of hydrodynamic erosion in turbulent flow. *Phys. Rev. Fluids*, *2*(11), 114302. doi: 10.1103/PhysRevFluids.2.114302

Schmeeckle, M. W. (2014). Numerical simulation of turbulence and sediment transport of medium sand. *Journal of Geophysical Research: Earth Surface*, *119*(6), 1240–1262.

Schmeeckle, M. W., & Nelson, J. M. (2003, April). Direct numerical simulation of bedload transport using a local, dynamic boundary condition. *Sedimentology*, *50*(2), 279–301. doi: 10.1046/j.1365-3091.2003.00555.x

Schumer, R., Meerschaert, M. M., & Baeumer, B. (2009). Fractional advection-dispersion equations for modeling transport at the earth surface. *Journal of Geophysical Research: Earth Surface*, *114*(F4).

Shields, A. (1936). Application of similarity principles and turbulence research to bed-load movement.

Shim, J., & Duan, J. (2019). Experimental and theoretical study of bed load particle velocity. *Journal of Hydraulic Research*, *57*(1), 62–74.

Shim, J., & Duan, J. G. (2017, March). Experimental study of bed-load transport using particle motion tracking. *Int. J. Sediment Res.*, *32*(1), 73–81. doi: 10.1016/j.ijsrc.2016.10.002

Slotterback, S., Mailman, M., Ronaszegi, K., van Hecke, M., Girvan, M., & Losert, W. (2012, February). Onset of irreversibility in cyclic shear of granular packings. *Phys. Rev. E*, *85*(2), 021309. doi: 10.1103/PhysRevE.85.021309

Sumer, B. M., Chua, L. H. C., Cheng, N.-S., & Fredsøe, J. (2003, August). Influence of Turbulence on Bed Load Sediment Transport. *J. Hydraul. Eng.*, *129*(8), 585–596. doi: 10.1061/(ASCE)0733-9429(2003)129:8(585)

Toiya, M., Stambaugh, J., & Losert, W. (2004). Transient and oscillatory granular shear flow. *Physical review letters*, *93*(8), 088001.

Turowski, J. M., Badoux, A., & Rickenmann, D. (2011, February). Start and end of bedload transport in gravel-bed streams. *Geophys. Res. Lett.*, *38*(4). doi: 10.1029/2010GL046558

Vericat, D., Batalla, R. J., & Garcia, C. (2006). Breakup and reestablishment of the armour layer in a large gravel-bed river below dams: The lower ebro. *Geomorphology*, *76*(1-2), 122–136.

Viterbi, A. (1967). Error bounds for convolutional codes and an asymptotically optimum decoding algorithm. *IEEE transactions on Information Theory*, *13*(2), 260–269.

Wang, D., Bodek, S., Ouellette, N. T., Shattuck, M. D., & O'Hern, C. S. (2026). Effect of sub-critical fluid shear flow on granular bed strength. *arXiv preprint arXiv:2604.14936*. doi: 10.48550/arXiv.2604.14936

Wiberg, P. L., & Smith, J. D. (1987). Calculations of the critical shear stress for motion of uniform and heterogeneous sediments. *Water resources research*, *23*(8), 1471–1480.

Wong, M., & Parker, G. (2006). Reanalysis and correction of bed-load relation of meyer-peter and müller using their own database. *Journal of Hydraulic Engineering*, *132*(11), 1159–1168.

Wu, Z., Furbish, D., & Foufoula-Georgiou, E. (2020). Generalization of hop distance-time scaling and particle velocity distributions via a two-regime formalism of bedload particle motions. *Water Resources Research*, *56*(1), e2019WR025116.

Yang, H., Hu, X., Wang, S., Cheng, K., Luo, M., Wang, H., & Shi, J. (2024, December). The effect of stress history on the critical shear stress of bedload transport in gravel-bed streams. *J. Hydrol.*, *645*, 132208. doi: 10.1016/j.jhydrol

.2024.132208